Engineered Science
DOI: https://dx.doi.org/10.30919/es1327

Size Effect of Gold Nanoparticles on the Photocatalytic Activity of Titanium Dioxide/Reduced Graphene Oxide (TiO_2/rGO) Nanocomposite

Timur Serikov,[1,*] Evgeniya Seliverstova[1,*] Aigul Sadykova,[1] Niyazbek Ibrayev[1] and Nurxat Nuraje[2, 3]

Abstract

A comparative study of the size effect of plasmonic nanoparticles on the photocatalytic activity of the titanium dioxide/reduced graphene oxide (TiO_2/rGO) nanocomposite material was performed. Gold (Au) plasmon nanoparticles with an average diameter of 20, 35, and 70 nm were embedded in the TiO_2/rGO nanocomposite material. It has been shown that the introduction of Au nanoparticles into the TiO_2/rGO structure leads to an increase in the absorption within the range from 475 to 600 nm. The best photocatalytic properties were recorded for the samples with 35 nm Au nanoparticles. These samples generated a photocurrent 2.3 times higher than pure TiO_2/rGO. In the presence of nanocomposite films, the photodegradation rate of the Methylene blue and Congo red dyes was increased by 3 and 2.6 times that of the sample without gold nanoparticles. The synergistic effect of plasmonic nanoparticles consists of the growth of the absorptivity of nanocomposite material, the reduction of its resistance, and the effective separation and transport of charge carriers, which leads to enhanced photocatalytic activity of semiconductors. The dependence of the photocatalytic activity of the TiO_2/rGO nanocomposite on the size of Au nanoparticles was explained by the hot electron injection cut off effect.

Keywords: TiO_2/rGO nanocomposite; Au nanoparticles; Size; Dye degradation; Photocatalysis.
Received: 29 September 2024; Revised: 14 November 2024; Accepted: 21 November 2024.
Article type: Research article.

1. Introduction

At present, humanity is faced with urgent problems, such as the elimination of environmental pollution and the generation of clean energy. Solar energy as one of the alternative energy resources, surpasses the planet's total energy demands.[1] With the help of solar energy, it is possible to obtain an environmentally friendly and economically profitable fuel-hydrogen and effectively purify water resources from various pollutants.[2,3] Such systems use various semiconductor photocatalysts, which have demonstrated themselves as promising materials for light harvesting and converting solar energy.[4,5] The main criteria for the selection of an effective photocatalyst are the location of their energy bands relative to the potential for splitting water and organic pollutants in water, inertness, non-toxicity, and low cost.[6-8] According to these criteria, the most suitable is the use of titanium dioxide (TiO_2) and its nanostructures. However, there are two key problems presented by TiO_2: firstly, the wide band gap of TiO_2 allows absorbing only ultraviolet (UV) light, which is no more than 7% in the solar spectrum; secondly is the high rate of charge recombination in TiO_2, which leads to insufficient photocatalytic activity.[9-13] One of the ways to eliminate the above disadvantages may be the preparation of heterostructure photoanode and the use of the phenomenon of localized plasmon resonance (LPR) of metal nanoparticles (NPs).[14-16]

In the case of LPR, a multiply enhanced optical and electric field is formed around the metal NPs, which accelerates the efficiency of photoinduced reactions. This effect is actively used in photodynamic therapy, biosensors, photonics,

[1] *Institute of Molecular Nanophotonics, Buketov Karaganda University, Karaganda, 100024, Kazakhstan.*
[2] *Department of Chemical and Materials Engineering, School of Engineering and Digital Science, Nazarbayev University, Astana, 010000, Kazakhstan.*
[3] *Renewable Energy Laboratory, National Laboratory Astana, Nazarbayev University, Astana, 010000, Kazakhstan.*
**Email:* genia_sv@mail.ru (E. Seliverstova), serikov-timur@mail.ru (T. Serikov)

optoelectronics, surface-enhanced Raman scattering (SERS), and catalysis.[17-19] Among the NPs of noble metals with LPR, gold NPs can be distinguished.[20] LPR of gold nanostructures has been used to increase the efficiency of dye-sensitized solar cells,[21] sensors and photodetectors,[22,23] and medicine.[24] However, it is especially impressive for the application of the plasmonic effect of gold NPs in photocatalytic systems.[25-31] In this case, several mechanisms are possible: when the surface of the gold NPs is illuminated, the plasmon can be re-emitted (scattered) and transfer energy to a semiconductor (PRET) or lead to the formation of hot electrons.[32] To determine the mechanism of the plasmon effect, it is necessary to know the size and shape of metal NP since the position and intensity of their absorptivity and scattering depend on them. In Ref. [33], Au NP of different sizes were synthesized and integrated into the @TiO_2 or @SiO_2 core-shell structures. It was shown that the degradation of salicylic acid is higher for Au@TiO_2 with Au diameters of 3 nm. When 17 nm Au NPs with a SiO_2 shell were added to the composites, they exhibited the best photocatalytic performance. The authors also investigated the effect of the Au NPs size on the photocatalytic degradation of the Methylene blue dye.[34] It was concluded that the enhancement of photodegradation is mainly due to the hot electron transfer and the interface structure. This means the photocatalytic efficiency is mainly influenced by the number of charge carriers and their transport rate at the semiconductor/metal interface. The influence of the shape of the Au NP on the photocatalytic activity of TiO_2 was discussed in Ref. [35]. The authors used nanospheres, nanostars, and Au nanorods. The phenol degradation was 3 times better in the presence of Au nanospheres than in TiO_2 and 1.5 and 2 times higher than for Au nanostars and nanorods.

In order to reduce charge recombination in a semiconductor, one could use composites containing graphene.[36-38] Introduction of graphene or graphene oxides into the TiO_2 structure improves the absorptivity of the material, promotes separation and transfer of charge carriers, and reduces the band gap,[39,40] contributing to an increase in the photocatalytic activity of the nanocomposite material. Due to the hydrophobicity of graphene, graphene oxides are more applicable since they have good solubility and stability in water and organic solvents.[41]

Currently, a sufficient number of scientific papers have been published on the study of the plasmonic effect of Au NPs on the photocatalytic activity of nanocomposite materials based on TiO_2 and reduced graphene oxide (rGO).[42-47] For example, the authors have developed a TiO_2/rGO photoelectrocatalyst with embedded Au NPs.[46] It has been established that the enhancement in catalytic activity is associated with the synergistic effect of the special microstructure of TiO_2 microspheres, improved light harvesting due to the LPR of Au NPs, effective charge separation, and rapid electron transfer through rGO nanosheets. The authors also found that the introduction of Au and rGO into TiO_2 makes it possible to increase the value of the active surface area of the semiconductor from 75 m^2g^{-1} to 135 m^2g^{-1}, which led to an increase in the degradation rate of the Methylene blue dye.[47] Earlier work demonstrated the effectiveness of triple Au/TiO_2/rGO nanocomposite materials in the photocatalytic water splitting reaction.[48] In such systems, Au NPs lead to the better absorption of visible light, rGO effectively reduces the rate of recombination, and one-dimensional electron transport along the walls of nanotubes promotes their participation in the photochemical reaction.

Despite these studies, the problem of the influence of the size of plasmon NPs on the characteristics of nanocomposites based on TiO_2 and reduced graphene oxide (rGO) remains open. In addition, in published works on the effect of the plasmon resonance of the Au NPs on the photocatalytic activity of the TiO_2/rGO nanocomposite, the sizes of the metal NP are studied only up to 17 nm.[49] Meanwhile, particles with a diameter of 20-50 nm are easier to synthesize. In addition, in metal NPs of a larger diameter, along with plasmon effects, light scattering should also be taken into account. In the present work, the photocatalytic and optical properties of the TiO_2/rGO nanocomposite in the presence of Au NPs of various diameters (20, 35 and 70 nm) are studied. It is assumed that due to the dependence of the position of the LPR band, the efficiency of absorption, extinction and scattering of plasmonic Au NP on their size, their effect on the semiconductor nanocomposite will differ.

As mentioned above, the properties of the plasmon resonance of Au NPs are determined not only by the size and shape of metal NP, but also by the methods of their preparation. In the above-mentioned works, colloidal or photosynthesis methods were used for the preparation of Au NPs. As a result, it is very difficult to obtain Au NPs without additional impurities with a controlled size and shape. In this regard, in the presented work, the method of laser ablation of a metal target (99.99%) in ethanol was used to obtain Au NPs. There will be no impurities in the NPs dispersions, and their sizes can be controlled by the power of laser radiation and the environment in which ablation occurs.[50-52]

2. Experimental section

2.1 Material preparation

The synthesis of TiO_2/rGO nanocomposite was performed according to the method described earlier in Refs [53,54]. For

this purpose, 20 mL of ethanol, 60 mL of deionized water, and 0.02 g of rGO (99 wt%, Cheaptubes) were sonicated (40 kHz, PS-10a) for 1 h. Then, 0.2 g of TiO_2 (<25 nm, Sigma Aldrich) was added to the solution and stirred for one more 1 hour in the ultrasonic bath and 1 h in a shaker (Multi Bio RS-24) until a homogeneous suspension was achieved. The suspension was then placed in an autoclave with a sealed Teflon container for 24 h (Snol, PL 20/12.5) at 120 °C to form the TiO_2/rGO composite material. After cooling to room temperature, the suspension was washed and filtered with deionized water and ethanol. The solution was then centrifuged at 4000.0 rpm. The resulting product was dried at 60 °C until all moisture was completely removed.

Au NPs were obtained by laser ablation of a gold target (99.999%) in ethanol using the second harmonic of neodymium-doped yttrium aluminum garnet (Nd:YAG) laser (LQ-215, SolarLS). The NPs concentration was estimated from the changes in the target's mass before and after ablation. The dynamic light scattering method with the Nanosizer S90 analyzer and Mark-Houwink equation in Zetasizer Software 7.10 (Malvern) was used to estimate the average diameter of Au NPs. As a result of varying the ablation's duration, Au NPs with the following characteristics were obtained (Table 1).

Table 1. Synthesis conditions, average diameters, and concentrations of Au NPs.

Duration of ablation (min)	Average diameter of the Au NPs (nm)	Concentration of Au NPs in ethanol (mol/L)	Sample designation of TiO_2/rGO+Au NPs
40	20 ± 10.6	2.3×10^{-11}	TGA_20
30	35 ± 10.0	2.3×10^{-11}	TGA_35
20	70 ± 11.1	2.1×10^{-11}	TGA_70

For the preparation of TiO_2/rGO nanocomposite paste, 0.150 g of TiO_2/rGO powder was stirred in 1 mL of ethanol for 24 h. After that, 2 mL of Au NPs (10^{-11} mol/L) in ethanol were added to the resulting paste and mixed for another 24 h. Thus, TiO_2/rGO pastes with the addition of Au NPs were obtained. Nanocomposite films from the prepared pastes were spin-coated (Polos Spin150i) at 3000 rpm on the surface of fluorine-doped tin oxide (FTO) substrates (1.5 × 1 cm^2, 7 Ohm/cm^2, Sigma–Aldrich). The thickness of the films ranges from 4 to 4.1 µm according to scanning electron microscopy (SEM) data. The TiO_2/rGO+Au NPs samples were designated as TGA-20, TGA-35, and TGA-70 for NPs with diameters of 20 ± 10.6, 35 ± 10.0 and 70 ± 11.1 nm, respectively.

2.2 Material characterization

The phase composition of the samples was studied using X-ray diffraction (XRD) patterns on an XRD diffractometer (Rigaku) with radiation from CuKα, λ=1.54060 Å. The X-ray spectra were analyzed using a database and the standard software package WinXPow. The morphology of the nanocomposite materials was studied with SEM Mira 3LMU (Tescan) with energy-dispersive analysis (EDA) capability. Transmission electron microscopy (TEM), high-resolution transmission electron microscopy (HRTEM) images, and selected area electron diffraction (SAED) patterns were obtained using a versatile transmission electron microscope JEM-1400 PLUS (Jeol) at an accelerating voltage of 120 kV. Before measurement, 0.001 g of the sample was sonicated in 2 mL of water for 20 minutes. The resulting suspension was then deposited on a copper grid (No. 01800, PELCO® TEM). The absorption spectra of the samples were recorded on a Cary 300 (Agilent).

The resistance and charge-transport properties of the samples were investigated using impedance spectroscopy in the frequency range from 1 MHz to 100 mHz. A Pt film (Platisol T/SP, Solaronix) deposited on the surface of an FTO substrate was used as the counter electrode. The electrodes were sealed with a 25 µm polymer film (Melotonix, Solaronix). Iodolyte Z-150 (Solaronix) was used as the electrolyte.

The photocatalytic activity was evaluated by measuring the photoinduced current over an illuminated area of 1 cm^2 using a potentiostat with an impedance spectra (EIS) analyzer (CS350, Corrtest Instruments) in a three-electrode setup, with AgCl and Pt foil electrodes. Measurements were conducted in 0.1 M NaOH electrolyte in a quartz container. Additionally, the photoactivity of the films was assessed by the photodegradation of the Methylene blue (MB) and Congo red (CR) dyes (10^{-5} mol/L) in aqueous solution. The dyes were used as model pollutants. A 300 W/cm^2 Xe lamp (Newport) was used as the light source in all experiments.

3. Results and discussion

The SEM images of Au NPs obtained by the laser ablation method are shown below (Fig. 1). Measurements revealed that after 20 minutes of Au target irradiation, the average diameter of the NPs was about 70 ± 11.1 nm. Additionally, particles with both larger and smaller diameters were present in the solution. When the ablation duration was increased to 30 minutes (see Fig. 1), the average diameter of the NPs was decreased to 35 ± 10.0 nm. After 40 minutes of irradiation, the NPs sizes further decreased to 20 ± 10.6 nm. Based on the obtained data, it can be inferred that the longer ablation results in the smaller diameter of the prepared Au NPs.

The synthesized Au NPs exhibit a broad band of absorption from 450 to 800 nm with a maximum at ~520-530 nm (Fig. 2). As the NPs diameter increases, the absorption maximum undergoes a bathochromic shift, corresponding to 520 nm, 530 nm, and 538 nm for 20 ± 10.6 nm, 35 ± 10.0 nm, and 70 ± 11.1 nm Au NPs, respectively. The absorption of Au NPs in the visible region is associated with the manifestation of LPR.

The obtained Au NPs were incorporated into the TiO_2/rGO nanocomposite. High-resolution TEM images (Fig. 3a) reveal that the TiO_2 particles are not aggregated and are predominantly located on the surface of the rGO nanosheets. As indicated by the authors in Ref. [55], this is a result of the interaction between the oxygen-containing groups of rGO and

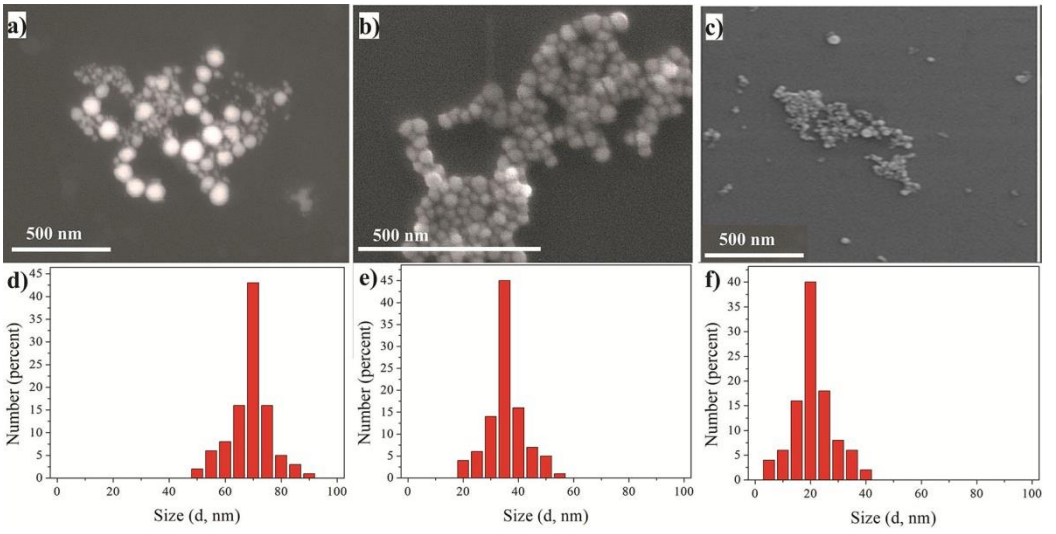

Fig. 1 SEM images and size distribution of Au NPs with various diameters: (a) and (d) 70 ± 11.1 nm; (b) and (e) 35 ± 10.0 nm; (c) and (f) 20 ± 10.6 nm.

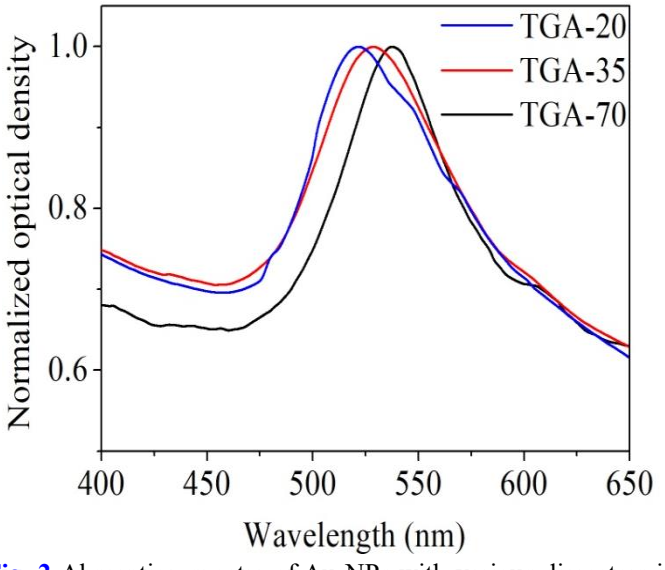

Fig. 2 Absorption spectra of Au NPs with various diameters in ethanol.

TiO_2. The HRTEM image, combined with the SAED pattern (Figs. 3b and 3c), further confirms the successful formation of the TiO_2/rGO nanocomposite. The image also reveals the presence of lattice fringes with an interplanar spacing of 0.35 nm, corresponding to the (101) plane of TiO_2 in the anatase modification. The SAED pattern shows that other peaks characteristic of the anatase modification, such as TiO_2 (200) and (211), are also present.

Similar studies were conducted for the TiO_2/rGO nanocomposite with Au NPs (sample TGA-35, Fig. 3d). The TiO_2 and Au NPs are primarily concentrated along the edges of the rGO nanosheets. The presence of lattice patterns with an interplanar spacing of 0.23 nm corresponds to the (111) plane of Au. The SAED images reveal characteristic rings of Au (planes (111) and (200)) and characteristic peaks of TiO_2 with anatase modification planes (200) and (101). EDA was performed to confirm the presence of the specified chemical elements in the composite materials (Figs. 3g and 3h). The spectra show the presence of Ti, O, and C for the TiO_2/rGO sample and, additionally, Au for the TGA-35 sample. The presence of Sn is likely due to the use of FTO substrates for the deposition of the nanocomposite films.

XRD analysis showed (Fig. 4a) that for TiO_2/rGO, most of the reflections correspond to the anatase modification of TiO_2. Reflections were recorded at 25.31°, 36.99°, 37.85°, 38.59°, 48.05°, 53.96°, 55.08°, 62.14°, 62.74°, 68.85°, 70.31°, 74.17°, 75.11°, 76.06°, 80.88°, 82.73°, and 83.19°, with the exception of a peak around 27°, which corresponds to the rutile modification with Miller index (101). It is important to note that almost all peaks match with the Joint Committee on Powder Diffraction Standards (JCPDS) database (card #01-070-7348). For Au NPs, XRD patterns should appear at 38.11°, 44.27°, 64.42°, and 77.47°. However, these reflections were not identified due to the low concentration of Au NPs and the overlap of some peaks with TiO_2 reflections. It is known that graphene oxide has only one peak, corresponding to the graphite plane with Miller index (001) around 10.5°. Nevertheless, it was not detected in the measured spectra due to the low concentration of rGO relative to TiO_2 and the high intensity of the latter's peaks.

The presence of rGO in the TiO_2/rGO nanocomposite was confirmed by Raman spectroscopy (Fig. 4b). In the spectra of the nanocomposite, Raman bands were observed with maxima at 1350 and 1590 cm^{-1}, corresponding to the D- and G-bands of rGO.[56] The crystalline structure of the anatase modification of TiO_2 is tetragonal. The unit cell consists of two primitive cells, each containing two blocks with a space group D 19/4h. According to group theory, anatase TiO_2 has six active Raman modes, which correspond to E_g mode at 144 cm^{-1}, E_g at 197 cm^{-1}, B_{1g} at 399 cm^{-1}, B_{1g} at 513 cm^{-1}, A_{1g} at 519 cm^{-1}, and E_g at 638.2 cm^{-1}.[57] However, in our studies, the peak at 197 cm^{-1} was not recorded due to its low intensity.

The maximum of the absorption of TiO_2/rGO is in the UV region at ~320 nm, with an absorption edge at ~380–400 nm

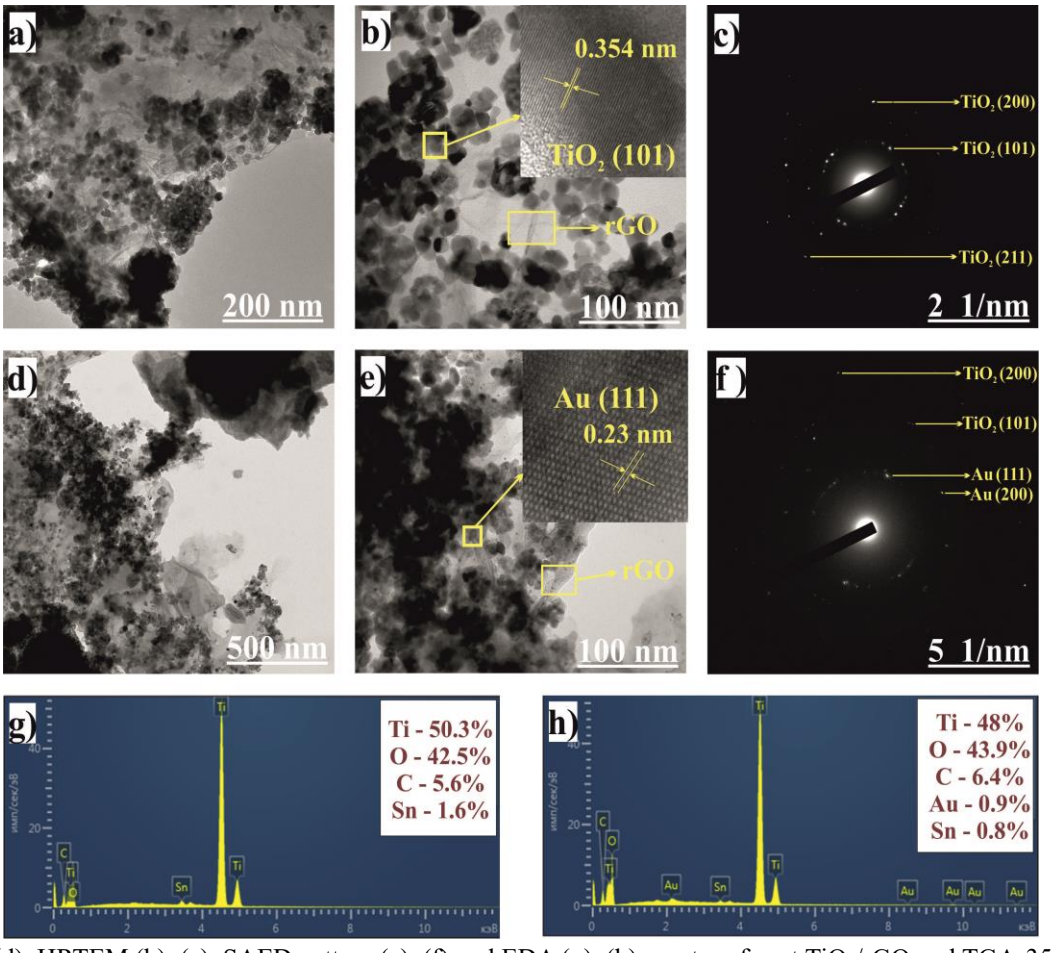

Fig. 3 TEM (a), (d), HRTEM (b), (e), SAED pattern (c), (f) and EDA (g), (h) spectra of neat TiO_2/rGO and TGA-35 samples.

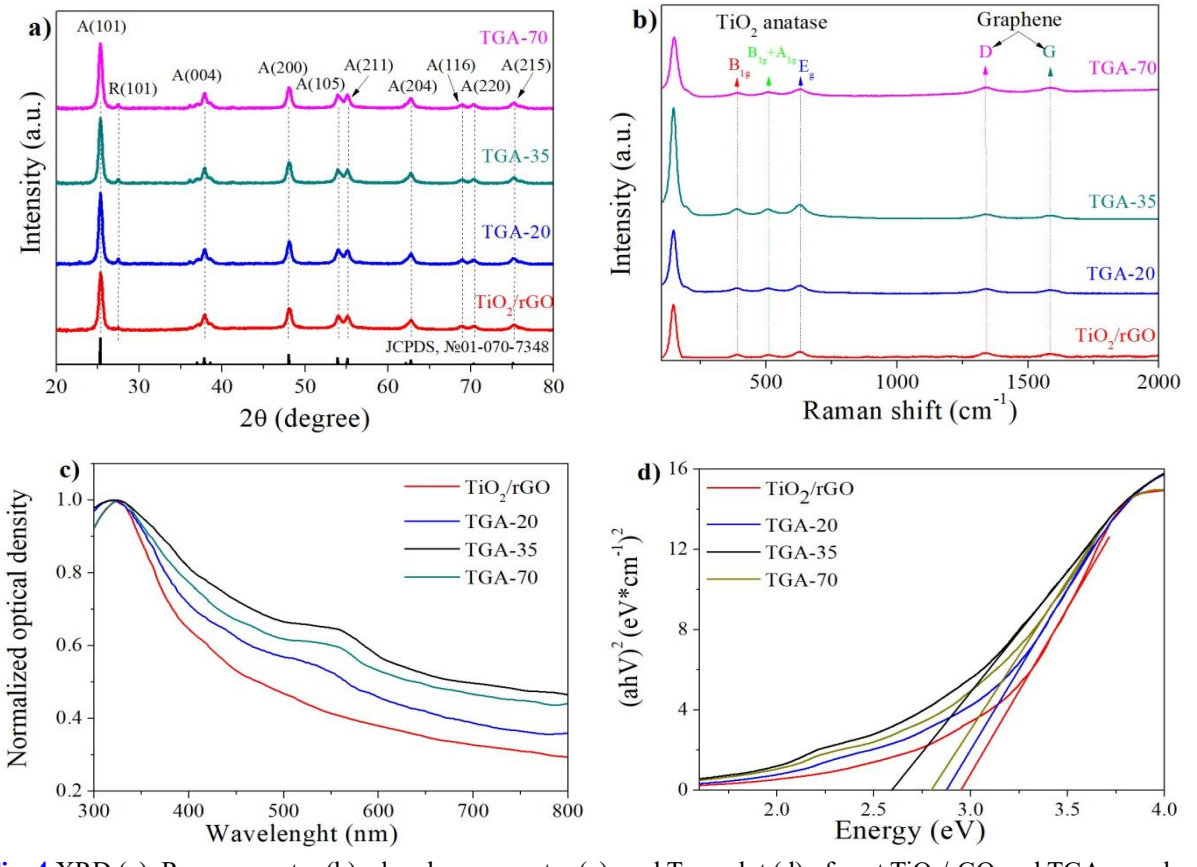

Fig. 4 XRD (a), Raman spectra (b), absorbance spectra (c), and Tauc plot (d) of neat TiO_2/rGO and TGA samples.

(Fig. 4c). When plasmon NPs were added to the nanocomposite, a weakly pronounced absorption appears at 520–540 nm, which coincides with the absorption of Au NPs. The observed bathochromic shift of the absorption of NPs in the semiconductor matrix relative to the spectra in ethanol may be associated with the dependence of the absorption of plasmon NPs on the properties of the environment. According to the Mie theory,[58,59] it follows that the polarizability of the metal NPs (α) is determined by the Clausius-Mossotti equation (Eq. (1)):

$$\alpha = 3\varepsilon_0 V\left(\frac{\varepsilon-\varepsilon_m}{\varepsilon+2\varepsilon_m}\right) \quad (1)$$

where ε_0 is the permittivity of vacuum, ε_m is the permittivity of the medium surrounding the NPs, ε is the permittivity of the metal NP, and V is the volume of spherical NP. Thus, it is clear that the polarizability of the NPs directly depends on the size of the NP and its permittivity. The imaginary part of the permittivity, in turn, determines the absorption of light in the metal NPs.

The Tauc method was used to determine the optical band gap of TiO_2 in the presence of rGO and plasmon NPs (Fig. 4d). The calculated value of the band gap of the semiconductor in the TiO_2/rGO nanocomposite is 2.94 eV; for TGA-20, TGA-35 and TGA-70 samples, it equal to 2.83, 2.60 and 2.76 eV. The narrowing of the band gap of the nanocomposite is a consequence of the disalignment of the Fermi level in the semiconductor under its doping with metal NPs.[60,61] A decrease in the band gap of the semiconductor and the presence of additional absorption in the visible region in the presence of plasmon NPs increases the light-harvesting properties of the TiO_2/rGO in the visible range of the spectrum. Reducing the band gap width of TiO_2 should contribute to the more efficient generation of electron-hole pairs in the nanocomposite and their participation in photocatalytic processes.

Two methods were used to evaluate the photocatalytic activity of nanocomposite materials: measurement of the photoinduced current of the film and monitoring of the photodegradation of MB and CR dyes. The measurements showed that in the absence of radiation, the photocurrent value for all samples is zero (Fig. 5a). When the light is turned on, the photocurrent value (I_{ph}) instantly increases to 17 μA/cm^2. The addition of Au NPs makes it possible to significantly increase the values of the generated photocurrent. The highest photocurrent value was recorded for the TGA-35 sample, where the I_{ph} is 2.3 times higher than for pure TiO_2/rGO. The photocurrent of TGA-20 and TGA-70 nanocomposites is lower than in TGA-35, but is still 1.5 and 1.7 times higher than for TiO_2/rGO, respectively.

An increase in the value of I_{ph} indicates the appearance of more free electrons in the nanocomposite, which can participate in photochemical reactions, for example, during the water splitting or purification of water from various organic pollutants. The photodegradation of MB and CR has shown similar results (Figs. 5b and 5c). The degradation of dyes was estimated from the changes in their optical density at the maximum of the absorption band of MB (662 nm) and CR (494 nm) according to the procedure described in Ref. [62]. It

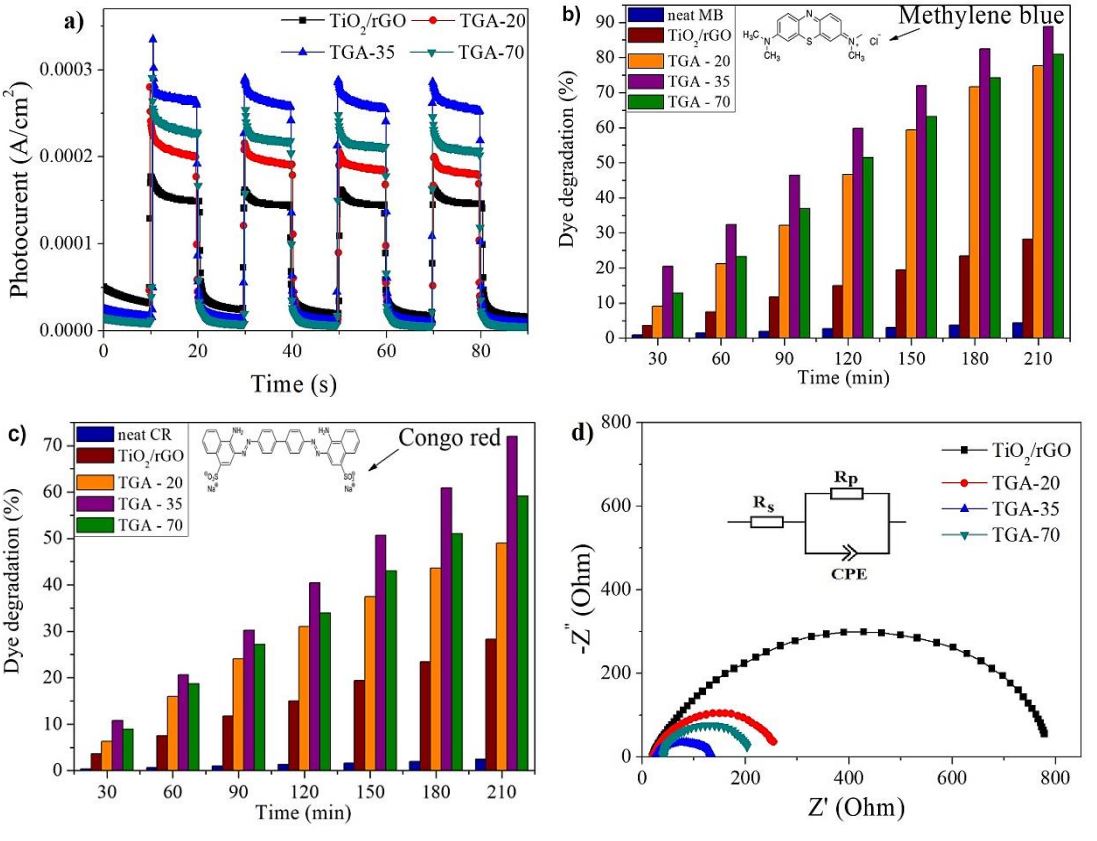

Fig. 5 Photocurrent (a), MB (b), and CR (c) dyes degradation and impedance spectra (d) of neat TiO_2/rGO and TGA samples.

can be seen from the presented data that upon prolonged irradiation of pure MB and CR solutions, their optical density changed slightly. However, the optical density, and therefore the dye concentration, was decreased when TiO_2/rGO films were immersed in a dye solution. It indicates the degradation of dyes. Moreover, the longer irradiation led to greater degradation for both MB and CR. The introduction of plasmon NPs into the TiO_2/rGO structure results in intensification of the photodegradation of dyes. The highest changes in dye concentrations were observed for dyes in the presence of a TGA-35 film. After 210 minutes of irradiation, the concentration of MB was decreased by 88% and CR by 77%, which is 3 and 2.6 times higher than in the sample without Au NPs. In the presence of TGA-20 and TGA-70 films, the degradation of MB and CR is lower than in TGA-35, but it is significantly higher than in TiO_2/rGO. This indicates that in the presence of Au NPs in the nanocomposite, a more efficient generation of charge carriers occurs, which are involved in the processes of photodegradation of organic dyes.

Impedance spectra in Nyquist coordinates of the nanocomposite samples without and with Au NPs are shown in Fig. 5d. Using the EIS spec software (Corrtest Instr.), a simple equivalent circuit was selected, taking into account the best fitting of the measured and modeled curves. In this case, the software calculates the value of the serial and parallel resistances and capacitances of the constant phase element (CPE). CPE is used to model non-ideal capacitive behavior in electrochemical systems or electronic circuits. In addition, using the calculation algorithm presented in Ref. [63], the effective electron lifetime (τ_{eff}) in a nanocomposite material was calculated using the central arc of the impedance spectra (Table 2). The value R_s characterizes the equivalent resistance of the film from the entire volume of the nanocomposite and the contact resistance between the layers. R_p simulates the resistance of charge carrier transfer at the interface of the studied layer with the electrode. As the results showed, the values of R_s resistances for all samples are almost identical and are in the confidence error range, which indicates that all assembled electrochemical cells are technologically identical. The value of the charge carrier transfer resistance (R_p) for TiO2/rGO is about 762 Ohms, which is 5 times higher than that for TGA-35 and 2.9 and 3.7 times higher than that for TGA-20 and TGA-70, respectively.

Table 2. Numerical values of calculations of electrophysical parameters of nanocomposite films obtained from impedance spectroscopy data.

Sample	R_s (Ohm)	CPE	R_p (Ohm)	τ_{eff} (s)
TiO_2/rGO	23.00	$1.92 \cdot 10^{-5}$	762.00	0.062
TGA-20	36.00	$3.97 \cdot 10^{-5}$	260.00	0.020
TGA-35	24.00	$2.93 \cdot 10^{-5}$	149.00	0.012
TGA-70	27.00	$3.58 \cdot 10^{-5}$	205.00	0.018

The effective electron lifetime in TGA-35 is 5 times less than in TiO_2/rGO, and 1.7 and 1.4 times less than in TGA-20 and TGA-70. This indicates that in the samples with Au NPs electrons reach the counter electrodes faster and more efficiently due to changes in resistance and improved charge transport in the volume of the nanocomposite. This contributes to the effective separation of electron-hole pairs, allowing them to participate in photocatalysis reactions.

In earlier works,[64-66] the mechanisms of enhanced photocatalytic properties of semiconductor materials in the presence of plasmon NPs were explained as increased optical absorption of a semiconductor due to LPR, injection of hot electrons from NPs into TiO_2 and resonant photon scattering. Much later, the mechanisms were supplemented in Ref. [67] in the quantum-mechanical approximation, where the LPR promotes electronic transitions from one to other states of the sp-band but with different electronic pulses, which correspond to intraband transitions. Hot electrons of Au NPs from intraband transitions have higher energy than the Fermi level and can be transferred to the empty states in reagents. The transferred electrons can activate chemical bonds by filling anti-binding orbitals. The stronger electronic bond between reagents and nanocrystals leads to an easier transition. Thus, the diffusion of hot carriers to the surface of semiconductor nanocrystals and their possible participation in the photocatalytic reaction play a decisive role in the growth of the catalytic efficiency of nanocomposites.

The dependence of the photocatalytic activity of the TiO_2/rGO nanocomposite on the size of Au NPs can be explained by the hot electron injection cut-off effect.[68] As shown above, the plasmon resonance spectrum of Au NPs shifts to the red region of the spectrum with an increase in the average diameter of NPs. Consequently, the NPs will absorb photons of lower energy, which could result in both a reduced number of generated hot electrons and their faster decay. This leads to a lower probability of hot electron injection into the semiconductor's conduction band and a smaller contribution to the recorded photocurrent. On the other hand, the relatively longer lifetime of hot electrons excited by photons of shorter wavelengths, as well as the higher energy of these electrons, allow more efficient separation of charge carriers at the metal NPs-semiconductor interface and their injection into TiO_2. It is reasonable to assume that the NPs size plays a significant role in this process. The dependence of the decay time of hot electrons on excitation energy and diameter has been demonstrated in Refs. [69,70] The decay time of hot electrons in NPs of small diameter (less than 20 nm) is shorter than in larger NPs. It was shown that the injection efficiency decreases with increasing particle volume for Au NPs with a diameter of more than 40 nm.[68,71,72] At the same time, NPs with a size of less than 10 nm have relatively low light absorption due to surface attenuation effects.[68,72] As the obtained data show, the most optimal ratio between the relaxation time of hot electrons and their energy is achieved in Au NPs with a diameter of 35 ± 10 nm.

In addition, it should be taken into account that plasmon NPs contribute to more efficient light harvesting by the

semiconductor due to their absorption in the visible region of the spectrum, as we showed earlier in Ref. [53]. The combination of efficient transfer of hot electrons from the NPs to the semiconductor and increased light absorption is manifested in the growth of the photocatalytic activity of the nanocomposite based on TiO_2 and rGO.

4. Conclusions

The effect of gold NPs of various diameters on the properties of the TiO_2/rGO nanocomposite material was studied. Au NPs with an average diameter of 20 ± 10.6 nm, 35 ± 10.0 nm, and 70 ± 11.1 nm were obtained by laser ablation. The NPs concentration in the nanocomposite was ~10^{-11} mol/L.

HRTEM images confirmed the successful formation of a TiO_2/rGO nanocomposite with Au NPs. Characteristic peaks of TiO_2 (101) and Au (111) with interplane distances of 0.35 and 0.23 nm were identified from the patterns of diffraction rings. XRD data showed that TiO_2 is mainly in anatase modification with minor inclusions of rutile. Raman spectroscopy has established six active Raman modes, which correspond to E_g, B_{1g}, A_{1g} modes for TiO_2 and Raman scattering peaks at 1350 and 1590 cm^{-1} corresponding to rGO. The measurement of the absorption spectra showed that the maximum peak of TiO_2/rGO absorption is in the UV region at ~320 nm. The absorption of Au NPs exhibits at 520 – 540 nm. The addition of plasmon NPs to the TiO_2/rGO improve the light-harvesting of the nanocomposite and reduce its band width from 2.94 to 2.60 eV.

The photocatalytic activity of the samples was estimated by measuring the photoinduced current of films and photodegradation of MB and CR dyes. It is shown that the addition of plasmon NPs to a semiconductor can significantly increase the photocurrent generated. The highest photocurrent value was observed for the samples with 35 ± 10.0 nm Au NPs. In this case the photocurrent values are 2.3 times higher than for pure TiO_2/rGO. The photodegradation of dyes repeats this trend. The resistance to charge carriers transfer for TiO_2/rGO is about 762 Ohms, which is 5 times more than for TGA-35 and 2.9 and 3.7 times more than TGA-20 and TGA-70, respectively. The effective electron lifetime in TGA-35 is 5 times less than that in TiO_2/rGO, 1.7 and 1.4 times less than in TGA-20 and TGA-70. This indicates that the introduction of Au NPs into TiO_2/rGO results in faster and more efficient electron transport in the volume of the nanocomposite, that contributes to the effective separation of electron-hole pairs, allowing them to participate in photocatalysis reactions.

The dependence of the photocatalytic activity of the TiO_2/rGO nanocomposite on the size of Au NPs can be explained by the hot electron injection cut-off effect. More detailed information on the manifestation of this effect can be obtained using the transient absorption method and quantum chemical calculations. The results of this work can be used for the development of photocatalysts with improved light-harvesting and electrophysical characteristics for use in photoelectrochemical cells, for hydrogen generation, photodegradation of organic compounds, *etc.*

Acknowledgements

This work was supported by the Science Committee of the Ministry of Science and Higher Education of the Republic of Kazakhstan, Grant No. AP14871956. This work has been also supported by the Targeted program of the Science Committee of the Ministry of Science and Higher Education of the Republic of Kazakhstan (Grant No. BR21882439).

Conflict of Interest

There is no conflict of interest.

Supporting Information

Not applicable.

References

[1] Q. Wang, K. Domen, Particulate photocatalysts for light-driven water splitting: mechanisms, challenges, and design strategies, *Chemical Reviews*, 2020, **120**, 919-985, doi: 10.1021/acs.chemrev.9b00201.

[2] H. Hou, X. Zeng, X. Zhang, Production of hydrogen peroxide by photocatalytic processes, *Angewandte Chemie International Edition*, 2020, **59**, 17356-17376, doi: 10.1002/anie.201911609.

[3] S. Abdimomyn, S. Malik, M. Skakov, Y. Koyanbayev, A. Miniyazov, F. Malchik, Hydrogen storage materials: promising materials for kazakhstan's hydrogen storage industry, *Eurasian Chemico-Technological Journal*, 2024, **26**, 113-132, doi: 10.18321/ectj1635.

[4] S. Nishioka, F. E. Osterloh, X. Wang, T. E. Mallouk, K. Maeda, Photocatalytic water splitting, *Nature Reviews Methods Primers*, 2023, **3**, 42, doi: 10.1038/s43586-023-00226-x.

[5] A. Meng, L. Zhang, B. Cheng, J. Yu, Dual cocatalysts in TiO_2 photocatalysis, *Advanced Materials*, 2019, **31**, 1807660, doi: 10.1002/adma.201807660.

[6] N. Goodarzi, Z. Ashrafi-Peyman, E. Khani, A. Z. Moshfegh, Recent progress on semiconductor heterogeneous photocatalysts in clean energy production and environmental remediation, *Catalysts*, 2023, **13**, 1102, doi: 10.3390/catal13071102.

[7] Y. Li, S. C. E. Tsang, Recent progress and strategies for enhancing photocatalytic water splitting, *Materials Today Sustainability*, 2020, **9**, 100032, doi: 10.1016/j.mtsust.2020.100032.

[8] R. Marschall, 50 years of materials research for photocatalytic water splitting, *European Journal of Inorganic Chemistry*, 2021, **2021**, 2435-2441, doi: 10.1002/ejic.202100264.

[9] V. Etacheri, C. Di Valentin, J. Schneider, D. Bahnemann, S. C. Pillai, Visible-light activation of TiO_2 photocatalysts: advances in

theory and experiments, *Journal of Photochemistry and Photobiology C: Photochemistry Reviews*, 2015, **25**, 1-29, doi: 10.1016/j.jphotochemrev.2015.08.003.
[10] K. K. Paul, P. K. Giri, Shape tailored TiO_2 nanostructures and their hybrids for advanced energy and environmental applications: a review, *Journal of Nanoscience and Nanotechnology*, 2019, **19**, 307-331, doi: 10.1166/jnn.2019.15778.
[11] N. Lu, M. Zhang, X. Jing, P. Zhang, Y. Zhu, Z. Zhang, Electrospun semiconductor-based nano-heterostructures for photocatalytic energy conversion and environmental remediation: opportunities and challenges, *Energy & Environmental Materials*, 2023, **6**, e12338, doi: 10.1002/eem2.12338.
[12] M. Pelaez, N. T. Nolan, S. C. Pillai, M. K. Seery, P. Falaras, A. G. Kontos, P. S. M. Dunlop, J. W. J. Hamilton, J. A. Byrne, K. O'Shea, M. H. Entezari, D. D. Dionysiou, A review on the visible light active titanium dioxide photocatalysts for environmental applications, *Applied Catalysis B: Environmental*, 2012, **125**, 331-349, doi: 10.1016/j.apcatb.2012.05.036.
[13] X. Kang, S. Liu, Z. Dai, Y. He, X. Song, Z. Tan, Titanium dioxide: from engineering to applications, *Catalysts*, 2019, **9**, 191, doi: 10.3390/catal9020191.
[14] T. M. Serikov, N. K. Ibrayev, T. M. Ivanova, S. V. Savilov, Influence of the hydrothermal synthesis conditions on the photocatalytic activity of titanium dioxide nanorods, *Russian Journal of Applied Chemistry*, 2021, **94**, 442-449, doi: 10.1134/s1070427221040030.
[15] T. M. Serikov, A. S. Kayumova, A. S. Baltabekov, L. F. Ilyina, P. A. Zhanbirbayeva, Photocatalytic activity of nanocomposites based on titania nanorods and nanotubes doped with Ag and reduced graphene oxide nanoparticles, *Nanobiotechnology Reports*, 2023, **18**, 207-215, doi: 10.1134/s2635167623700040.
[16] T. M. Serikov, P. A. Zhanbirbayeva, A. S. Baltabekov, A. B. Kuanyshbekova, Photocatalytic activity of the TIO2/Ag/rGO nanocomposite, *Bulletin of the Karaganda University Physics Series*, 2022, **108**, 14-21, doi: 10.31489/2022ph4/14-21.
[17] N. Qutub, P. Singh, S. Sabir, S. Sagadevan, W.-C. Oh, Enhanced photocatalytic degradation of Acid Blue dye using CdS/TiO_2 nanocomposite, *Scientific Reports*, 2022, **12**, 5759, doi: 10.1038/s41598-022-09479-0.
[18] Q. Wang, H. Li, X. Yu, Y. Jia, Y. Chang, S. Gao, Morphology regulated Bi_2WO_6 nanoparticles on TiO_2 nanotubes by solvothermal Sb^{3+} doping as effective photocatalysts for wastewater treatment, *Electrochimica Acta*, 2020, **330**, 135167, doi: 10.1016/j.electacta.2019.135167.
[19] K. Khurana, N. Jaggi, Localized surface plasmonic properties of Au and Ag nanoparticles for sensors: a review, *Plasmonics*, 2021, **16**, 981-999, doi: 10.1007/s11468-021-01381-1.
[20] C. Díaz, M. Segovia, M. L. Valenzuela, Solid state nanostructured metal oxides as photocatalysts and their application in pollutant degradation: a review, *Photochem*, 2022, **2**, 609-627, doi: 10.3390/photochem2030041.
[21] M. Ijaz, Plasmonic hot electrons: potential candidates for improved photocatalytic hydrogen production, *International Journal of Hydrogen Energy*, 2023, **48**, 9609-9619, doi: 10.1016/j.ijhydene.2022.11.251.
[22] Y. Zhang, S. He, W. Guo, Y. Hu, J. Huang, J. R. Mulcahy, W. D. Wei, Surface-plasmon-driven hot electron photochemistry, *Chemical Reviews*, 2018, **118**, 2927-2954, doi: 10.1021/acs.chemrev.7b00430.
[23], F. Parveen, C. V. Jagtap, M. V. T, Copper nanoparticles incorporated titanium dioxide photoanode for plasmonic dye sensitized solar cell, *ES General*, 2024, **5**, 1163, doi: 10.30919/esg1163.
[24] Z. Bian, T. Tachikawa, P. Zhang, M. Fujitsuka, T. Majima, Au/TiO_2 superstructure-based plasmonic photocatalysts exhibiting efficient charge separation and unprecedented activity, *Journal of the American Chemical Society*, 2014, **136**, 458-465, doi: 10.1021/ja410994f.
[25] E. H. Peters, M. Mayor, Monofunctionalized gold nanoparticles: fabrication and applications, *CHIMIA*, 2021, **75**, 414, doi: 10.2533/chimia.2021.414.
[26] K. Khurana, N. Jaggi, Localized surface plasmonic properties of Au and Ag nanoparticles for sensors: a review, *Plasmonics*, 2021, **16**, 981-999, doi: 10.1007/s11468-021-01381-1.
[27] S. Sarina, E. R. Waclawik, H. Zhu, Photocatalysis on supported gold and silver nanoparticles under ultraviolet and visible light irradiation, *Green Chemistry*, 2013, **15**, 1814, doi: 10.1039/c3gc40450a.
[28] N. Chander, A. F. Khan, E. Thouti, S. K. Sardana, P. S. Chandrasekhar, V. Dutta, V. K. Komarala, Size and concentration effects of gold nanoparticles on optical and electrical properties of plasmonic dye sensitized solar cells, *Solar Energy*, 2014, **109**, 11-23, doi: 10.1016/j.solener.2014.08.011.
[29] S. K. Srivastava, V. Arora, S. Sapra, B. D. Gupta, Localized surface plasmon resonance-based fiber optic U-shaped biosensor for the detection of blood glucose, *Plasmonics*, 2012, **7**, 261-268, doi: 10.1007/s11468-011-9302-8.
[30] A. J. Jwar, U. M. Nayef, F. A. H. Mutlak, Study effect of magnetic field on $Au-TiO_2$ core–shell nanoparticles via laser ablation deposited on porous silicon for photodetector, *Plasmonics*, 2023, **18**, 595-605, doi: 10.1007/s11468-023-01791-3.
[31] A. Guglielmelli, F. Pierini, N. Tabiryan, C. Umeton, T. J. Bunning, L. De Sio, Thermoplasmonics with gold nanoparticles: a new weapon in modern optics and biomedicine, *Advanced Photonics Research*, 2021, **2**, 2170027, doi: 10.1002/adpr.202170027.
[32] L. T. M. Huynh, S. Kim, S. Yoon, Effect of material and shape of nanoparticles on hot carrier generation, *ACS Photonics*, 2022, **9**, 3260-3267, doi: 10.1021/acsphotonics.2c00530.
[33] S. M. Yoo, S. B. Rawal, J. E. Lee, J. Kim, H.-Y. Ryu, D. W. Park, W. I. Lee, Size-dependence of plasmonic Au nanoparticles in photocatalytic behavior of Au/TiO_2 and $Au@SiO_2/TiO_2$, *Applied Catalysis A: General*, 2015, **499**, 47-54, doi: 10.1016/j.apcata.2015.04.003.
[34] L. Lin, Q. Zhong, Y. Zheng, Y. Cheng, R. Qi, R. Huang, Size effect of Au nanoparticles in $Au-TiO_{2-x}$ photocatalyst, *Chemical*

Physics Letters, 2021, **770**, 138457, doi: 10.1016/j.cplett.2021.138457.
[35] A. Gołąbiewska, A. Malankowska, M. Jarek, W. Lisowski, G. Nowaczyk, S. Jurga, A. Zaleska-Medynska, The effect of gold shape and size on the properties and visible light-induced photoactivity of Au-TiO_2, *Applied Catalysis B: Environmental*, 2016, **196**, 27-40, doi: 10.1016/j.apcatb.2016.05.013.
[36] A. Nasir, S. Khalid, T. Yasin, A. Mazare, A review on the progress and future of TiO_2/graphene photocatalysts, *Energies*, 2022, **15**, 6248, doi: 10.3390/en15176248.
[37] N. T. Padmanabhan, N. Thomas, J. Louis, D. T. Mathew, P. Ganguly, H. John, S. C. Pillai, Graphene coupled TiO_2 photocatalysts for environmental applications: a review, *Chemosphere*, 2021, **271**, 129506, doi: 10.1016/j.chemosphere.2020.129506.
[38] E. V. Kachina, N. V. Ivanova, Y. A. Zakharov, G. Y. Simenyuk, Z. R. Ismagilov, M. V. Lomakin, Electrochemical properties of the composites based on multiwall carbon nanotubes modified with nanoparticles of mixed cobalt and nickel hydroxides, *Eurasian Chemico-Technological Journal*, 2022, **24**, 115, doi: 10.18321/ectj1323.
[39] B. Gupta, A. A. Melvin, TiO_2/RGO composites: its achievement and factors involved in hydrogen production, *Renewable and Sustainable Energy Reviews*, 2017, **76**, 1384-1392, doi: 10.1016/j.rser.2017.03.123.
[40] J. Corredor, M. J. Rivero, I. Ortiz, New insights in the performance and reuse of rGO/TiO_2 composites for the photocatalytic hydrogen production, *International Journal of Hydrogen Energy*, 2021, **46**, 17500-17506, doi: 10.1016/j.ijhydene.2020.01.181.
[41] L. Zhang, Q. Zhang, H. Xie, J. Guo, H. Lyu, Y. Li, Z. Sun, H. Wang, Z. Guo, Electrospun titania nanofibers segregated by graphene oxide for improved visible light photocatalysis, *Applied Catalysis B: Environmental*, 2017, **201**, 470-478, doi: 10.1016/j.apcatb.2016.08.056.
[42] M. Sharma, K. Behl, S. Nigam, M. Joshi, TiO_2-GO nanocomposite for photocatalysis and environmental applications: a green synthesis approach, *Vacuum*, 2018, **156**, 434-439, doi: 10.1016/j.vacuum.2018.08.009.
[43] S. Sagadevan, K. Pal, P. Koteeswari, A. Subashini, Synthesis and characterization of TiO_2/graphene oxide nanocomposite, *Journal of Materials Science: Materials in Electronics*, 2017, **28**, 7892-7898, doi: 10.1007/s10854-017-6488-3.
[44] A. Zhumabekov, N. Ibrayev, E. Seliverstova, Photoelectric properties of a nanocomposite derived from reduced graphene oxide and TiO_2, *Theoretical and Experimental Chemistry*, 2020, **55**, 398-406, doi: 10.1007/s11237-020-09632-8.
[45] H. M. El-Bery, Y. Matsushita, A. Abdel-moneim, Fabrication of efficient TiO_2-RGO heterojunction composites for hydrogen generation via water-splitting: comparison between RGO, Au and Pt reduction sites, *Applied Surface Science*, 2017, **423**, 185-196, doi: 10.1016/j.apsusc.2017.06.130.
[46] M. Saquib, R. Kaushik, A. Halder, Photoelectrochemical activity of Ag coated 2D-TiO_2/RGO heterojunction for hydrogen evolution reaction and environmental remediation, *ChemistrySelect*, 2020, **5**, 6376-6388, doi: 10.1002/slct.202000843.
[47] R. Boppella, S. T. Kochuveedu, H. Kim, M. J. Jeong, F. Marques Mota, J. H. Park, D. H. Kim, Plasmon-sensitized graphene/TiO_2 inverse opal nanostructures with enhanced charge collection efficiency for water splitting, *ACS Applied Materials & Interfaces*, 2017, **9**, 7075-7083, doi: 10.1021/acsami.6b14618.
[48] S. A. Balsamo, R. Fiorenza, M. T. A. Iapichino, F. J. Lopez-Tenllado, F. J. Urbano, S. Sciré, H_2 production through glycerol photoreforming using one-pot prepared TiO_2-rGO-Au photocatalysts, *Molecular Catalysis*, 2023, **547**, 113346, doi: 10.1016/j.mcat.2023.113346.
[49] H. An, H. Wang, S. Fang, M. Li, X. He, L. Zhao, Z. Yin, Design and optimization of photocatalytic performance of 3D TiO_2 microspheres through Au nanoparticles and rGO co-modification, *Materials Research Express*, 2019, **6**, 075026, doi: 10.1088/2053-1591/ab1426.
[50] N. Ben Saber, A. Mezni, A. Alrooqi, T. Altalhi, Fabrication of efficient Au@TiO_2/rGO heterojunction nanocomposite: boosted photocatalytic activity under ultraviolet and visible light irradiation, *Journal of Materials Research and Technology*, 2021, **12**, 2238-2246, doi: 10.1016/j.jmrt.2021.03.109.
[51] M. De Anda Villa, J. Gaudin, D. Amans, F. Boudjada, J. Bozek, R. Evaristo Grisenti, E. Lamour, G. Laurens, S. Macé, C. Nicolas, I. Papagiannouli, M. Patanen, C. Prigent, E. Robert, S. Steydli, M. Trassinelli, D. Vernhet, A. Lévy, Assessing the surface oxidation state of free-standing gold nanoparticles produced by laser ablation, *Langmuir*, 2019, **35**, 11859-11871, doi: 10.1021/acs.langmuir.9b02159.
[52] L. S. De Bortoli, C. R. Vanoni, C. L. Jost, D. Z. Mezalira, M. C. Fredel, Stable and ligand-free gold nanoparticles produced by laser ablation as efficient electrocatalysts for electrochemical sensing of dopamine, *Journal of Electroanalytical Chemistry*, 2023, **947**, 117744, doi: 10.1016/j.jelechem.2023.117744.
[53] E. Seliverstova, T. Serikov, N. Nuraje, N. Ibrayev, A. Sadykova, M. Amze, Plasmonic effect of metal nanoparticles on the photocatalytic properties of TiO_2/rGO composite, *Nanotechnology*, 2024, **35**, 325401, doi: 10.1088/1361-6528/ad3e02.
[54] E. Seliverstova, T. Serikov, A. Sadykova, N. Ibrayev, N. Nuraje, Enhanced photocatalytic properties of TiO_2/rGO nanocomposites Doped with CdS, *Materials Letters*, 2025, **379**, 137660, doi: 10.1016/j.matlet.2024.137660.
[55] N. Ben Saber, A. Mezni, A. Alrooqi, T. Altalhi, Fabrication of efficient Au@TiO_2/rGO heterojunction nanocomposite: boosted photocatalytic activity under ultraviolet and visible light irradiation, *Journal of Materials Research and Technology*, 2021, **12**, 2238-2246, doi: 10.1016/j.jmrt.2021.03.109.
[56] J. H. Byeon, Y. W. Kim, Gas-phase self-assembly of highly ordered Titania@Graphene nanoflakes for enhancement in photocatalytic activity, *ACS Applied Materials & Interfaces*, 2013, **5**, 3959-3966, doi: 10.1021/am400765z.
[57] A. A. Melvin, P. A. Bharad, K. Illath, M. P. Lawrence, C. S. Gopinath, Is there any real effect of low dimensional morphologies towards light harvesting? A case study of Au–rGO-

TiO_2 nanocomposites, *ChemistrySelect*, 2016, **1**, 917-923, doi: 10.1002/slct.201600182.
[58] S. A. Maier, Plasmonics: fundamentals and applications, 2007.
[59] W. Hergert, T. Wriedt, The Mie Theory Basics and Application, 2012.
[60] S. A. Anjugam Vandarkuzhali, N. Pugazhenthiran, R. V. Mangalaraja, P. Sathishkumar, B. Viswanathan, S. Anandan, Ultrasmall plasmonic nanoparticles decorated hierarchical mesoporous TiO_2 as an efficient photocatalyst for photocatalytic degradation of textile dyes, *ACS Omega*, 2018, **3**, 9834-9845, doi: 10.1021/acsomega.8b01322.
[61] V. Subramanian, E. E. Wolf, P. V. Kamat, Catalysis with TiO_2/gold nanocomposites. effect of metal particle size on the Fermi level equilibration, *Journal of the American Chemical Society*, 2004, **126**, 4943-4950, doi: 10.1021/ja0315199.
[62] S. W. Ko, H. Chung, Preparation of C60 fullerene nanowhisker–CuS nanoparticle composites and photocatalyst for rhodamine B degradation under blue light emitting diode irradiation, *Eurasian Chemico-Technological Journal*, 2023, **25**, 65, doi: 10.18321/ectj1496.
[63] M. Adachi, M. Sakamoto, J. Jiu, Y. Ogata, S. Isoda, Determination of parameters of electron transport in dye-sensitized solar cells using electrochemical impedance spectroscopy, *The Journal of Physical Chemistry B*, 2006, **110**, 13872-13880, doi: 10.1021/jp061693u.
[64] K. Qian, B. C. Sweeny, A. C. Johnston-Peck, W. Niu, J. O. Graham, J. S. DuChene, J. Qiu, Y. C. Wang, M. H. Engelhard, D. Su, E. A. Stach, W. D. Wei, Surface plasmon-driven water reduction: gold nanoparticle size matters, *Journal of the American Chemical Society*, 2014, **136**, 9842-9845, doi: 10.1021/ja504097v.
[65] Y. C. Pu, G. Wang, K. D. Chang, Y. Ling, Y. K. Lin, B. C. Fitzmorris, C. M. Liu, X. Lu, Y. Tong, J. Z. Zhang, Y. J. Hsu, Y. Li, Au nanostructure-decorated TiO_2 nanowires exhibiting photoactivity across entire UV-visible region for photoelectrochemical water splitting, *Nano Letters*, 2013, **13**, 3817-3823, doi: 10.1021/nl4018385.
[66] L. Qin, G. Wang, Y. Tan, Plasmonic Pt nanoparticles-TiO_2 hierarchical nano-architecture as a visible light photocatalyst for water splitting, *Scientific Reports*, 2018, **8**, 16198, doi: 10.1038/s41598-018-33795-z.
[67] P. Lyu, R. Espinoza, S. C. Nguyen, Photocatalysis of metallic nanoparticles: interband vs intraband induced mechanisms, *The Journal of Physical Chemistry C*, 2023, **127**, 15685-15698, doi: 10.1021/acs.jpcc.3c04436.
[68] M. Lickleder, R. Mohammadi, N. T. Nguyen, H. Park, S. Hejazi, M. Halik, N. Vogel, M. Altomare, P. Schmuki, Dewetted Au nanoparticles on TiO_2 surfaces: evidence of a size-independent plasmonic photoelectrochemical response, *The Journal of Physical Chemistry C*, 2019, **123**, 16934-16942, doi: 10.1021/acs.jpcc.9b02769.
[69] N. Ibrayev, E. Seliverstova, M. Kucherenko, Features of nanosecond transient absorption of Ag nanoparticles with manifestations of electron gas degeneracy, *Journal of Luminescence*, 2022, **245**, 118760, doi: 10.1016/j.jlumin.2022.118760.
[70] N. K. Ibrayev, E. Seliverstova, A. Kanapina, Transient absorption of gold nanoparticles of various diameters, *Eurasian Physical Technical Journal*, 2022, **19**, 73-77, doi: 10.31489/2022no4/73-77.
[71] M. Valenti, M. P. Jonsson, G. Biskos, A. Schmidt-Ott, W. A. Smith, Plasmonic nanoparticle-semiconductor composites for efficient solar water splitting, *Journal of Materials Chemistry A*, 2016, **4**, 17891-17912, doi: 10.1039/c6ta06405a.
[72] N. Wu, Plasmonic metal–semiconductor photocatalysts and photoelectrochemical cells: a review, *Nanoscale*, 2018, **10**, 2679-2696, doi: 10.1039/c7nr08487k.